**Article type:** Paper

**Title** Fabrication of Silicon Nanopillar Arrays by Electron Beam Lithography and Reactive Ion Etching for Advanced Bacterial Adhesion Studies

*P. W. Doll*, A. Al-Ahmad, A. Bacher, A. Muslija, R. Thelen, L. Hahn, R. Ahrens, B. Spindler, E. Hellwig, A. E. Guber*

Patrick W. Doll, Andreas Bacher, Alban Muslija, Richard Thelen, Dr. Lothar Hahn, Dr. Ralf Ahrens, Prof. Andreas E. Guber
Karlsruhe Institute of Technology, Institute of Microstructure Technology, Hermann-von-Helmholtz-Platz 1, 76344 Eggenstein-Leopoldshafen, Germany
E-mail: patrick.doll@kit.edu

Prof. Ali Al-Ahmad, Prof. Elmar Hellwig
Medical Center - Department of Operative Dentistry and Periodontology – Faculty of Medicine, University of Freiburg -, Hugstetter Straße 55, 79106 Freiburg, Germany

Dr. Bruno Spindler
Fräszentrum Ortenau GmbH & Co KG, Industriestr. 2-4, 77728 Oppenau, Germany

Keywords: nanopillars, electron beam lithography, reactive ion etching, bacterial adhesion, biomaterial associated infections

## Abstract

Within this work we demonstrate the fabrication of silicon nanopillar arrays for advanced cell/surface interaction studies and the results of the bacterial interaction of *Escherichia coli* with such highly ordered nanostructures.

By combination of Electron Beam Lithography and Reactive Ion Etching a powerful and highly precise method for the fabrication of nanopillars with different diameters in the sub 100 nm region and high aspect ratios is available. The fabrication method allows building highly ordered nanotopographies which can help to increase the understanding of cell/substrate interaction. The biological results indicate that the adhesion of *E. coli* correlates to the available discrete adhesion bond points on top of the pillars and additionally that the cells align with the nanostructures to maximize their contact to the surface.

The research of such structures will lead to the development of novel materials which might reduce biomaterial associated infections.

## 1. Introduction

Biomaterial-associated infections are caused by a wide range of bacteria and have serious consequences in different medical and surgical fields [1]. Hence there is an urgent need for strategies to prevent bacterial adhesion to material surfaces. Especially the early stage of adhesion, the initial bacterial adhesion, is the first step of the formation of highly resistant biofilms [2, 3]. Nanostructures like nanopillars e.g. are currently under broad discussion to be able to reduce bacterial adhesion or even to kill bacteria on contact to the surface [4-7]. Those structures are widely known in other applications, especially in optics and photonics [8-11]. The fabrication of such structures can be realized using different methods reaching from random based approaches [12, 13] to more challenging ones like the so called Inductively Coupled Plasma (ICP) method [4, 14, 15] or to fully controlled electron beam lithography based methods [16, 17].

The so called black silicon consists of randomly distributed pillar like nanostructures [12]. These pillars form within a reactive ion etching (RIE) process containing $SF_6$ as a coincidence of random partly passivation of the surface and a simultaneous etching between these passivated spots [12]. Typical diameters of the pillars are 50-100 nm and the height varies depending on the etching time [7, 12].

The ICP method instead is a more challenging approach where a monolayer of e.g. glass or gold nano beads is applied to a substrate surface. This monolayer of beads can act as an etch mask in further processing. The intermediate area between the beads can be etched by reactive ion etching thus forming pillars. However due to errors in bead monolayer alignment as well as variation in bead size distribution etc. the resulting pillars are not completely homogenous and the arrangement pattern has various errors [4, 14, 15].

These random or bead based methods deliver more or less highly varying results in respect to pillar profile geometry, uniformity, height, control of distances etc. and thus the overall quality of the surface topography on the nanoscale.

The most accurate fabrication method available is the direct structuring of an electron sensitive photoresist layer on top of a substrate by Electron Beam Lithography (EBL). The structured resist layer can be used as an etch mask and an additional anisotropic Reactive Ion Etching step allows the precise fabrication of various kinds of nanostructures [16, 17].

The fabrication of nanostructures by EBL and RIE is well known in nanotechnology yet the implementation of these methods for microbiologic research like advanced cell substrate interaction studies is insufficient. Cell adhesion studies with highly ordered nanostructures are quite rare most likely due to the restricted availability and the high costs for the necessary machines and therefore such structures. Additionally the large amount of samples needed for adequate significant biologic results is another important issue which increases the total costs further.

To overcome this issue often only a master structure is fabricated by EBL and RIE and copies of that master are then produced by different casting techniques like Nano Imprint Lithography, Hot Embossing and so on [18-20]. Those techniques themselves are quite challenging in respect to uniformity and minimal form error especially if the structures are becoming smaller [18-19]. For subsequent mass replications the molds are then replicated with a photoresist or PDMS for example. This quick reproduction cycle is the main advantage of the processes.

But even small changes in sample/feature geometry require that the whole fabrication process has to be repeated completely, significantly slowing down further progress. Another issue with replication techniques is the structure fidelity. The replicated samples often show a lack in detail due to incomplete infiltration of the material into the mold, sticking of material to the sidewall or even whole structure parts are not replicated at all due to local clogging of the molds [19].

But often the lack of detail and limitations to only a few different geometries limits further understanding in advanced cell substrate interactions. The way how bacteria interact with their environment is still not fully understood [5, 21-25].

Often the effects of nanostructures on cell adhesion are misinterpreted due to limitations in surface metrology [5, 6]. But the knowledge of the exact surface topography is crucial for understanding the adhesion mechanisms on the nanoscale. In this case especially the usage of descriptive figures like the average roughness value $R_a$ is not reasonable at all since very different surface topographies can have same $R_a$ values. In particular, the interaction of cells with surfaces requires a more detailed view of surface metrology and must be further established [5, 6]. In addition to the lack of knowledge about the exact surface topography the effect of random based nanoscopic features are often misunderstood. Often the overall arrangement of the features effect cells on a micrometer- and not on a nanometer-scale [5, 6]. To overcome these current limitations and to help answer these basic questions nanotechnology is a promising field, both in precise surface metrology including the knowledge of real surface topography and the fabrication of adequate model surfaces with nanometer precision. Only with such adequate nanotopographies we will be able to build descriptive models for the interaction of cells with their environment and it might allow us to engineer novel antibacterial biomaterials.

We believe that it is necessary to use discrete and highly ordered nanotopographies to investigate cell adhesion. Our goal is to make this knowledge about fabrication more public to reduce further cost intensive production/setup times. The presented electron lithography based method allows the fabrication of different highly ordered nanopillar arrays hopefully resulting in a better availability for other researchers and increasing further research for advanced cell/substrate interaction studies.

## 2. Material and Methods

The fabrication of nanostructures by Electron Beam Lithography (EBL) and Reactive Ion Etching (RIE) consists of several individual steps.

In general the process is similar to other lithographic processes like UV-lithography. As substrates silicon, glass or even metals like titanium can be used. The substrate is coated with an electron beam sensitive photo resist. Structures are then exposed into that layer of photo resist by a focused electron beam. Depending on the tone of the photo resist either the exposed or the unexposed areas of the resist can be removed after exposure by development. After that step we have a substrate covered with a nanostructured resist layer which could be used on its own if it fulfills the necessary requirements in respect to the material requirements. If e.g. higher aspect ratios are needed a following etching step can be applied to copy the nanostructured resist layer into the base material. This is usually achieved by anisotropic etching processes like RIE.

### 2.1. Substrates

First 4" Silicon wafers of 525 µm thicknesses, (CZ, P/B doped, <100>, Siegert Wafer, Germany) were cut into 20 x 20 mm chips (DAD3430 Dicing Saw, Disco, Japan). To avoid particle contamination on the surface a protection layer for dicing of AR-N 7520.12 (Allresist, Germany) was applied by spin coating with 2000 rpm, 1500 rpm/s for 60 s (Opticoat, ATM, Germany). After spin coating a hotbake step at 90 °C was performed to evaporate the remaining solvent. The wafers were then placed "sunny side down" on the cutting machine holders consisting of a clamp ring with clamped adhesive tape. The wafers were cut into 20 x 20 mm pieces of which 12 can be further used for processing. After cutting the wafer was placed on a custom-built heat spreader and the cut chips were spread all around to be able to pick up individual chips without producing additional particles. The chips were ultrasonically cleaned in acetone which also removed the protection layer, 2-propanol and DI-water for 10 min respectively. Afterwards the chips were blow dried with compressed

nitrogen. For handling a special wafer tweezer with polymer tips was used. The described cleaning procedure was always performed directly before coating. All work has been carried out in cleanroom conditions (equal to or better than ISO 5).

**2.2. Coating**

Before spin coating procedure the chips were dry baked at 180 °C to evaporate any possible remaining water layer on the surfaces for at least 5 min. During this time all chips were placed on a dummy silicon wafer which was placed on a hotplate. After a cooling period of around 60-80 s one chip was coated with the negative tone electron sensitive photo resist Hydrogen Silsesquioxane (HSQ) with a solids concentration of 6% (Dow Chemical, USA) [26, 27]. Parameters for spin coating were 4000 rpm, 1500 rpm/s for 60 s. A softbake step at 95°C for 60 s was carried out to evaporate the remaining solvent. This procedure was repeated for all chips which had to be processed within one batch of fabrication. The produced resist layers have average thicknesses of 137 ± 2 nm. The thickness was measured using an ellipsometer after softbake (Sentech Pro, Sentech, Germany). For circular structures with diameters below 100 nm a thinner resist layer was used. It was also applied by spin coating HSQ but with only 2% solids concentration. Parameters were 3000 rpm, 1500 rpm/s, 60s and this procedure delivered 45.9 ± 0.37 nm thick resist layers.

Since HSQ is highly sensitive to oxygen atmosphere and tends to crosslink quickly therefore limiting possible resolution, the time to vacuum was kept as low as possible and always stayed below 40 min for this work. Within the Ultra High Vacuum (UHV) of the Electron Beamwriter the photo resist layers are stable for a few days and probably even longer. Still exposure of the samples was performed as soon as possible after coating.

**2.3. Electron Beam Lithography**

EBL was carried out on a state of the art E-Beam Pattern Generator (EBPG5200Z, Raith, Netherlands). The machine allows the exposure of substrates of up to 8” with an Extra High Tension (EHT) of 100 kV, a Clock Timing of up to 125 MHz and minimal feature sizes of

even less than 5 nm [28, 29]. To show the ability of the system for the use with cutting edge structure fabrication for biologic interaction studies we fabricated different structures and different structure field sizes. The 20 x 20 mm silicon chips were mounted on a special sample holder. For biological interaction studies firstly circular patterns with field sizes of 500 x 500 µm were created. Additionally line structures of different widths to show the procedures potential were also fabricated. In a final step we increased the field sizes of the 100 nm circular patterns by a factor of 100 from 500 x 500 $\mu m^2$ (0.25 $mm^2$) to 5000 x 5000 $\mu m^2$ (25 $mm^2$) enabling better biological results or even the use of bigger cells like eukaryotic cell lines. Since the necessary dose which has to be applied for full exposure of the electron sensitive resist is e.g. dependent on the type of photo resist, lateral structure size, resist thickness, substrate material, structure pattern etc. the correct dose for a new layout has to be determined. To identify the optimal doses a dose variation test was performed using a broad range of different doses ranging from 500 up to 13000 $\mu C/cm^2$ depending on the layout patterns. The final 100 nm circular structures were written using a Beam Step Size (BSS) of 5 nm and a Beam Current (BC) of 8 nA which results in a beam diameter of approx. 8 nm. For field sizes of 5000 x 5000 $\mu m^2$ a BSS of 20 nm and a BC of 30 nA were used. This increase of BSS and BC is necessary to achieve shorter total exposure times. Finally the 20 and 50 nm circular patterns were written using a BSS of 2 nm and a BC of 2 nA with a dose of 10500, 11500, 12500 $\mu C/cm^2$ for 20 nm and 8000, 9000 and 10000 $\mu C/cm^2$for the 50 nm respectively.

**2.4. Development**

Following exposure, the samples have been developed within a maximum of 6 h to avoid further cross linking of the resist due to exposure to oxygen-containing atmosphere. This would reduce the possible contrast and reduce the overall quality of the geometric shape of the structures. For development one chip at a time was placed in a custom PTFE holder and immersed into a beaker containing 25% Tetramethylammonium hydroxide (TMAH) solution

(Sigma Aldrich, Germany). The beaker was placed on a shaking plate (200 rpm) and the development was performed for 120 s. An over development of the structures is unlikely as even a development time of 8 min does not change the result at all. As reported by others the process is self-limiting meaning an over development is unlikely to occur due to a passivating layer on the HSQ surface [30, 31]. After the TMAH development the holder containing the chip was removed and immediately rinsed with 2-propanol for at least 30 s. It was additionally rinsed with DI-water for another 30 s and blow dried with compressed nitrogen. This cleaning step is crucial for high contrast and mask quality. If the residues are not removed immediately they can form cross links between the structures. An additional hard bake step can be performed to fully crosslink the remaining HSQ resulting in a complete glass like surface without the presence of Silicon-Hydrogen Bonds [32]. After development the geometry and size of the circles have been analyzed using Scanning Electron Microscopy (SEM) and Atomic Force Microscopy (AFM).

**2.5. Reactive Ion Etching**

To copy the written nanostructures into the silicon base material a dry etching step was performed using a Cryo Reactive Ion Etching process [33]. The process takes place within an ICP etcher (Oxford Plasmalab 100/ICP 380, Oxford Instruments, England) at a temperature of -110°C. As reaction gas-mixture a combination of 20 sccm $SF_6$, 10 sccm $O_2$ and 10 sccm Ar was used. Within the process a part of the gases is ionized within the plasma creating $F^-$ and $O^-$ radicals and $SF_5^+$. Due to the low temperatures a deposit of a combination of the $SF_5^+$, $F^-$ and $O^-$ takes places creating a passivation layer protecting the sample from being etched further [33]. By acceleration of the reaction-gases and -particles and the argon ions towards the sample within the ICP a partly removal of this passivating layer takes place at the upmost areas while the sidewalls of the mask and the substrate remain passivated. This allows the precise etching of complete perpendicular structures. By diminishing plasma power to a minimum a more precise erosion of the material can take place. At 750 W ICP and 100 W Rf

power an etch rate of ~ 20 nm/s can be achieved. If the power is further reduced the plasma will not stay stable.

The complete etching procedure can be divided into four steps: Firstly a cooling step is performed after loading the samples which were placed on a carrier wafer and thermally connected with a thin layer of Perfluoropolyether (PFPE) between chip and carrier wafer into the ICP chamber. A cooling time of 5 min is used to be sure that a temperature of -110°C is reached. After the cooling step the ignition step takes place in which the reaction gases are introduced into the plasma chamber and the plasma is ignited at a slightly higher power of 1000 W ICP. In the next step which is the main etch step the plasma power is reduced just above the possible limit to decrease the etch rate allowing a more precisely erosion. After etching for 25 s the plasma is turned off and a purge step with argon is performed to remove the reaction gases.

After etching the samples were removed from the carrier wafer and the bottom side was cleaned with 2-propanol. After this process all samples are rinsed with acetone followed by 2-propanol and DI-water respectively. For bacterial tests each 20 x 20 $mm^2$ chip was diced into 4 individual 10 x 10 $mm^2$ chips, each containing one nano patterned field of 500 x 500 $\mu m^2$ size. The glass mask was not removed.

**2.6. Bacterial Adhesion Tests**

*2.6.1. Strain and culture conditions*

*Escherichia coli* ATCC 25922 was used for adhesion experiments. The strain was cultivated on Columbia Blood (CoBl; Oxoid, Germany) agar plates at 37°C and 5-10 % $CO_2$, for the overnight cultures and the inoculation in Trypticase soy broth (TSB) bouillon (Oxoid, United Kingdom). The bacterial strain was maintained routinely with weekly subculturing on Columbia blood agar. Long term storage of these bacteria has been conducted at -80°C in basic growth medium containing 15 % v/v glycerol as described in [34].

*2.6.2. Inoculation and colonization*

Inoculation and colonization were conducted as described earlier in detail with some modification [35]. The overnight culture was grown in TSB at 37°C water bath (GFL, Germany) with permanent stirring. 50 ml cell suspensions of each overnight culture were centrifuged at 2000xg for 10 min (Hettich, Germany). The supernatants were removed and 50 ml TSB were added. 100 µl of each organism were streaked onto CoBl agar plates which were incubated for two days at 37°C and 5-10% $CO_2$ (HeraCell, Thermo Scientific Heraeus, Germany) in order to determine the number of colony forming units (CFUs) present in each overnight culture. The optical densities of the bacterial solutions were measured at 595 nm (Bio-Rad, Life Science Group, Hercules, USA) against TSB as a blank. The CFUs number of overnight culture was in the range of 108-109/ml corresponding to an optical density in the range of 1.2-1.5. Four samples of each material were placed into wells of multiwell plates (24 well plate, Greiner Bio-One, Germany). Then 1 ml of bacterial suspension was added to each well and the samples were incubated at 37°C for two hours and 24 hours, respectively, with constant swirling. For the 24 hours incubation the bacterial cultures were removed after 12 hours and a fresh bacterial culture medium was added to the samples. After the incubation period the probes were rinsed two times with saline solution (0.9%, Braun, Germany) to remove the non-adherent microorganisms. For SEM analysis the material samples with adherent bacteria were fixed in 8% formaldehyde for three days.

For examination by Scanning Electron Microscopy (SEM), the samples inoculated with bacteria were fixed in 8 % formaldehyde for three days at 4 °C and dehydrated in graded alcohol (30 %, 50 %, 70 %, 80 %, 90 %, one time each and twice in 99.8 % for 1 h). After critical point drying (Critical Point Dryer CPD 030, Bal-Tec, Wallruf, Germany) using liquid carbon dioxide according to standard procedure, the samples were examined.

16 images per sample were taken covering the sample surface in an equal pattern. A Secondary Electron 2 (SE2) Detector with an EHT of 3 kV was used at working distances of 3-6 mm.

*2.6.3. Quantitative Analyses*

For capturing the quantitative data for bacterial colonization and adhesion ability on to the nanopillar array structures 16 individual and non-overlapping images have been taken with SEM for each individual sample. The cells on each image have been counted using the graphics software ImageJ. The data has been prepared and statistically analyzed (one-way-ANOVA and Turkey´s test) with the statistics program Origin (OriginLab, USA).

*2.6.4 Cell Orientation Analysis*

One interesting question within the interaction of the cells with their environment is the orientation of the cells to or between features as reported by others [36, 37]. One can expect that rod shaped cells like *E.coli* align to the pillar grid sitting on top of the pillar heads or between two rows of pillars. To visualize that behavior the orientation of the longitudinal axis of the rod shaped *E. coli* were analyzed using the graphics software ImageJ. For that each acquired SEM image for the 2 h incubation time was analyzed and the rotation angle of each single cell was measured. The rotation angle of single bacteria can be described as an angle between 0°-90°. For comparison the range from 0°-90° was equally divided into 30 groups of 3° each.

**2.7. Characterization**

*2.7.1. Scanning Electron Microscopy (SEM)*

SEM analysis of the samples was performed using an EHT of 3 kV at different working distances ranging from 4.5 to 6.5 mm (Supra VP 60, Zeiss, Germany). For quantitative analysis a magnification of 2000 x has been used. For additional images different magnifications and EHT-values were used. The SEM is placed inside a cleanroom to allow intra fabrication analysis without leaving the cleanroom.

*2.7.2. Atomic Force Microscopy (AFM)*

Structured samples have been analyzed with Atomic Force Microscopy (Dimension Icon, Bruker, USA) to characterize the pillar head shape, diameter and height. Analysis was carried

out in Tapping Mode with special High Aspect Ratio Tips (TESPA-HAR Bruker AFM Probes, Bruker, Germany). These tips are specially designed to measure high aspect ratio structures and have tip heights of 10-15 µm, front, back and side angles of 5° and a tip radius of approx. 10 nm. The tips have a spring constant of 42 N/m and a resonance frequency of 320 kHz. The selected high aspect ratio design allows the penetration of the interpillar space and therefore the detection of the substrate bottom between individual pillars.

*2.7.3. Contact Angle Measurements*

Contact angle Measurements were carried out after fabrication of the samples using the sessile drop method and a droplet volume of 4 µl of deionized water (OCA50, Data Physics, Germany). The droplet was carefully placed on top of the structures. 3 measurements per sample were taken to build a representative value for this topography. Measurement procedure was kept strictly for each measurement to reduce variance by evaporation, air flow or operator.

*2.7.4. Surface Roughness*

Surface roughness is calculated after **Equation 1** with h being the height of the pillars, r the radius and d the grid width of the equidistant hexagonal pattern. Since the main influence for the average roughness value comes from the height and the area covered by the pillars this formula is applicable. Yet it explanatory power is limited. The roughness value for the flat reference sample was measured by AFM with a field of view of 10 x 10 µm$^2$ at three random positions within one sample with the previously described scanning parameters.

$$R_a(\mathrm{d}) = \frac{\frac{\mathrm{h}}{2}\pi r^2}{\frac{\mathrm{d}^2\sqrt{3}}{4} - \frac{1}{2}\pi r^2} \quad (1)$$

## 3. Results and Discussion

### 3.1. Fabrication of Nanopillar Arrays

**Figure 1** shows an example of the fabricated 100 nm High Aspect Ratio nanopillars. It is important that fabrication runs smoothly. Essential for the whole process is the coating step and the fast transition to UHV. If the coated samples are kept under normal atmosphere for too long the HSQ layer starts to crosslink limiting possible resolution and contrast drastically and therefore reducing the overall sample quality. The quality may be reduced even up to a degree were it cannot be processed any further. One extremely time consuming step is the identification of optimal dose and optimal write strategy in respect to the beam current, beam step size etc. which is needed for the individual type of structures and arrangements/patterns of those structures. To provide this information to others the complete optimized writing strategy and the necessary parameters for reproducing these structures are listed in **Table 1**. While minimizing the BC and the BSS generally delivers the best results in profile geometry, the necessary writing time rises drastically. 100 nm pillars can even be produced with a bigger BC of 30 nA resulting in an approx. beam diameter of 25 nm and a BSS of 20 nm. Doing so delivers adequately round circles without any bigger deformations to be observed by SEM. One main crucial part in EBL is the necessary total exposure time since E-Beam exposure time is very expensive due to machine cost, maintenance, cleanroom supply etc. In case of 100 nm pillars, hexagonally arranged with total field sizes of 500 x 500 $\mu m^2$ optimized total exposure times of approx. 11, 7 and 5 min for interpillar distances of 200, 300 and 400 nm respectively could be achieved. To show the influence and the necessity of optimization on writing time we increased the field size to 5 x 5 $mm^2$, thus increasing the net area of one field of nanostructures by a factor of 100. Such field sizes can be used for further advanced microbiological evaluation like determination of CFU after initial adhesion etc.

**Table 1:** List of complete EBL parameters for fabrication of nanopillars with diameters of 100 nm.

| Fieldsize [mm$^2$] | Grid [nm] | BSS [nm] | BC [nA] | Dose [µC/cm$^2$] | ~Time [min] |
|---|---|---|---|---|---|
| 0.25 | 200 | 5 | 8 | 3000 | 11 |
| | 300 | | | 4500 | 7 |
| | 400 | | | 5500 | 5 |
| 25 | 200 | 20 | 30 | 3000 | 135 |
| | 300 | | | 4500 | 90 |
| | 400 | | | 5500 | 80 |

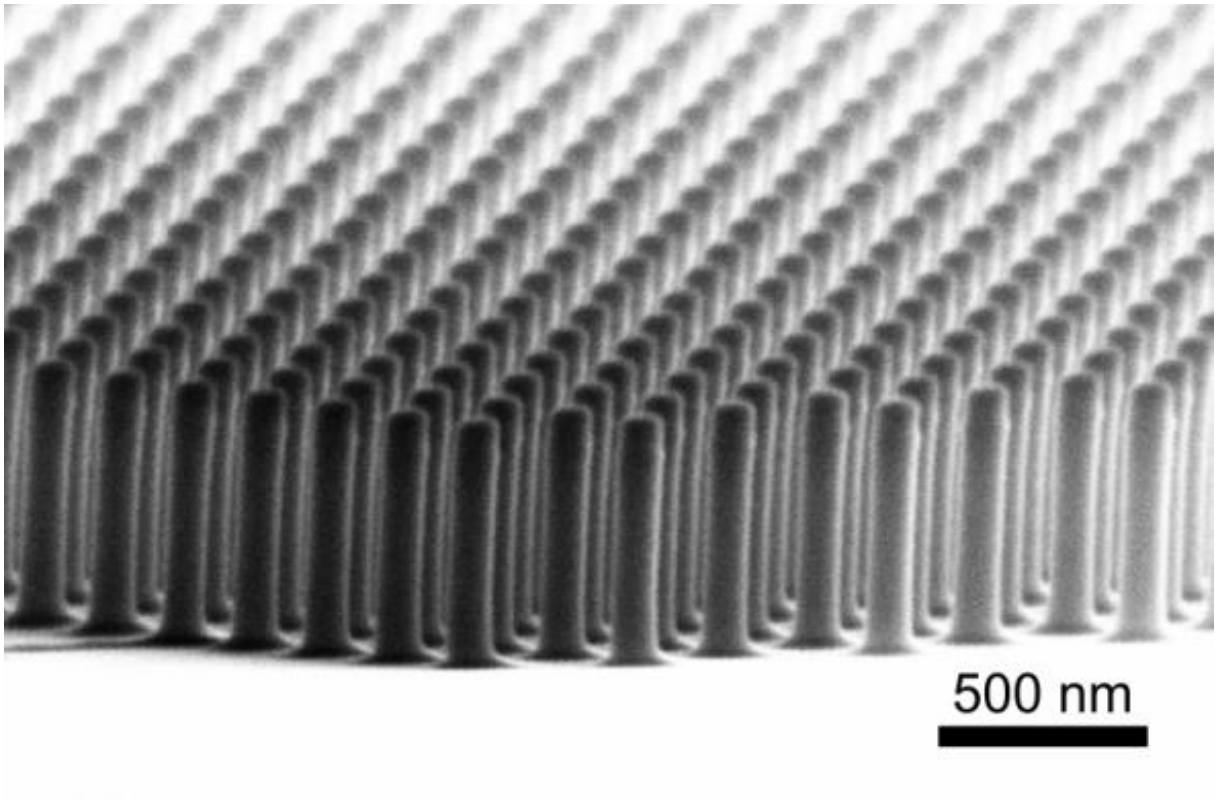


**Figure 1:** Scanning Electron Micrograph of a tilted sample containing highly ordered nanopillars arranged hexagonally in a 200 nm grid. The HSQ/glass mask is still visible on the top of the pillars as indicated by a slightly darker color.

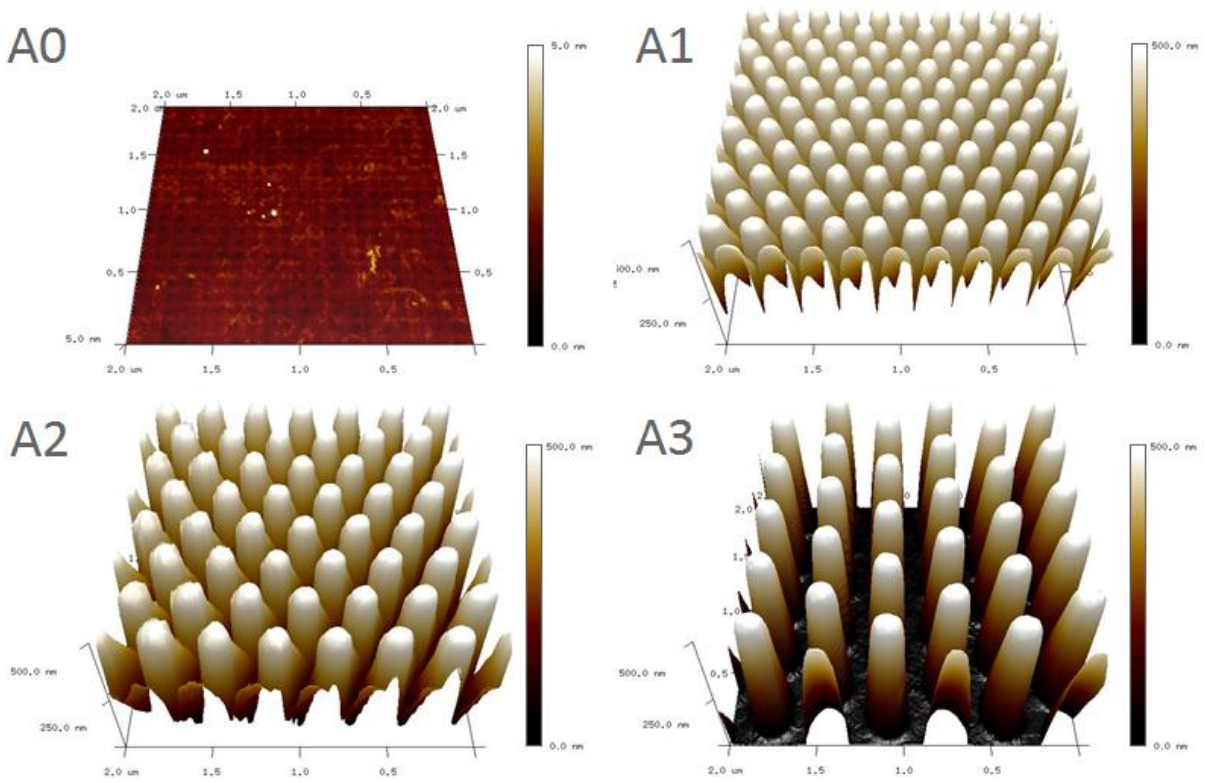


**Figure 2:** Representative height profile visualizations of the different nanopillar arrangements acquired by Atomic Force Microscopy measurements. A0: flat reference, A1, 200 nm grid, A2: 300 nm grid. A3: 400 nm grid.

As an example we started producing 500 x 500 µm$^2$ fields with a non-optimized strategy with a BSS of 2 nm and a BC of 5 nA which takes approx. 52 min to expose a single field of 100 nm pillars arranged in a hexagonal pattern with an interpillar distance of 200 nm.

The area of that field is 0.25 mm$^2$ and consists of approx. 3.6 x 10$^6$ individual nanopillars. Increasing field size to 25 mm$^2$ results in an increase of the total number of pillars by a factor of 100 and the necessary total exposure time would increase to approx. 5200 min respectively. By applying optimized exposure parameters that exposure will only take approx. 135 min which is a drastic reduction of the exposure time allowing the samples to be produced in a decent amount of time and therefore with much lower costs.

Since surface roughness is often told to have a major influence on bacterial adhesion the roughness values of the samples which were used for the bacterial tests were calculated and correlating AFM measurements were taken to determine the average roughness for the flat

HSQ reference sample (**Figure 2**). Additionally contact angle measurements showed a super hydrophobic behavior for the nanostructures (**Table 2**). The average roughness for the nanopillar structures was calculated by Equation 1 which is principally applicable since the structures are completely optimized in diameter and form and the whole structure fields are without larger defects. Yet the average roughness value does not deliver further information about the real sample surface topography. Instead it is misleading making the sample with the largest pillar distance (A3) the smoothest. Instead of the simple average roughness a more detailed view using summit density ratio e.g. can be applied to further describe the surface topography and the interaction with bacteria [6]. The roughness for the flat reference sample was measured by AFM with a scan field of 10 x 10 $\mu m^2$ and shows a very flat average surface roughness. All roughness values and contact angles are displayed in Table 2.

**Table 2:** Average Roughness Values [$R_a$] and Contact Angles for nanopillars of 100 nm diameter.

| | **A0** | **A1** | **A2** | **A3** |
|---|---|---|---|---|
| Interpillar distance [nm] | flat | 200 | 300 | 400 |
| $R_a$ [nm] | 0.58 ± 0.03* | 146,6 | 56 | 30 |
| Contact angle [°] | 87 ± 1.3 | 133 ± 2.6 | 121 ± 1.5 | 112 ± 2.6 |

*Measurement by AFM

Contact angle measurements show that the flat reference shows a slightly hydrophilic behavior while the nanopillars structures show an expected super hydrophobic behavior. The contact angle slightly decreases while the distance between the nanopillars is increased.

In addition to circular structures/pillars with diameters of 100 nm also 50 and even 20 nm circles and pillars have been created. **Figure 3** shows the results of EBL of the 50 and the 20 nm circular pattern. **Table 3** shows the corresponding write strategies for EBL for 50 and 20 nm circles arranged in hexagonal grids.

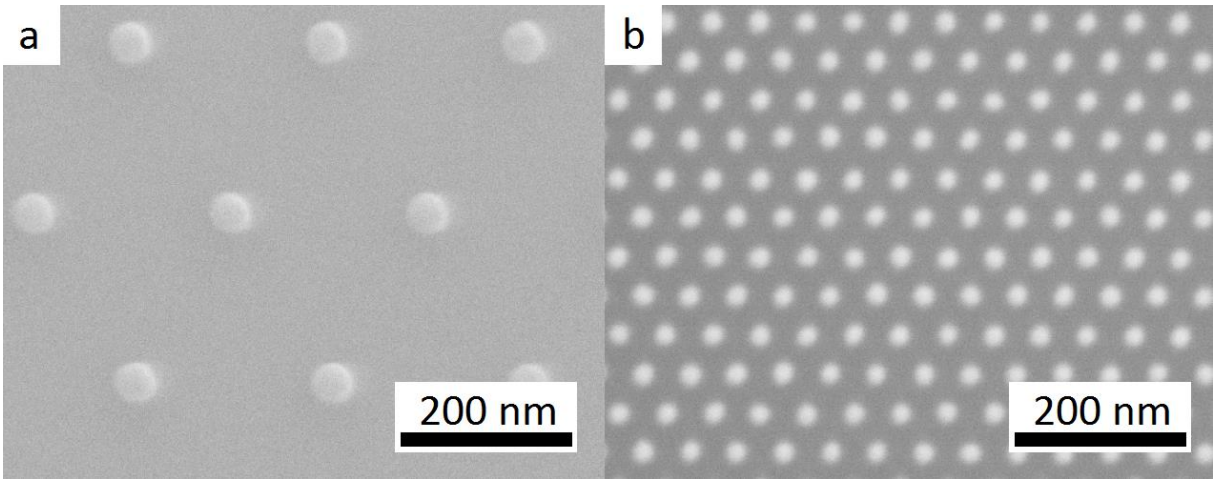


**Figure 3**: Scanning Electron Micrograph images of samples containing (a) 50 nm and (b) 20 nm circles which have been made by EBL. The circles consist of glass-like material HSQ.

**Table 3:** List of complete EBL parameters for fabrication of nanopillars with diameters of 50 and 20 nm (field size of 500 x 500 µm$^2$).

| diameter [nm] | Grid [nm] | BSS [nm] | BC [nA] | Dose [µC/cm$^2$] | ~Time [min] |
|---|---|---|---|---|---|
| 50 | 100 | 2 | 5 | 8000 | 32.4 |
| | 200 | | | 9000 | 18.8 |
| | 300 | | | 10000 | 13.5 |
| 20 | 100 | 2 | 5 | 10500 | 31.8 |
| | 150 | | | 11500 | 16.5 |
| | 250 | | | 12500 | 7.3 |

### 3.2. Bacterial Tests

Within this work we demonstrate the influence of a nanotopography in form of highly ordered silicon based nanopillars on the bacterial adhesion of rod shaped *E. coli* bacteria. Classic CFU determination could not be performed because a sonication step would destroy the nanostructured samples. Instead a quantitative assay for the colonization ability of *E. coli* on nanopillars was used as an indication of cell adhesion after washing off non-adherent cells [4]. It can be assumed that the number of cells that irreversibly stick to the surface can be directly correlated to the adhesion strength of the cells to the surface. Therefore a reduction of adherent cells would indicate a reduction of adhesion strength and vice versa.

Though real adhesion forces have not yet been measured within this work this method should indicate the differences in adhesion strength of the different nanostructured surface so a relative comparison is possible.

Since the pillar distances are smaller than the diameter of the cells an interaction can only takes place on the pillar heads and only there tight bonds between the cells and the surface can be generated. If this correlation is applied to the adhesion of the cells it can be assumed that a reduction of that top layer contact area will result in a reduction of the adhesion and therefore the number of adherent cells. The red line in **Figure 5** shows the correlation between the nanopillar array pattern geometry and the available contact area. It is obvious that by increasing the grid size the available contact area decreases respectively. The curve is normalized to the structure geometry A1 (200 nm) as 100 %. By simply limiting the possible contact area it should therefore be possible to reduce the number of adherent cells.

As a further result of the influence of the fabricated nanostructures on the cell adhesion and cell substrate interaction, the cell orientation on top of the pillars was analyzed. It should show a discrete orientation of the cells to or between the pillars like others have reported in general [36, 37].

*3.2.1. Quantitative Cell Analysis*

Cell counts show a correlation between the pattern geometry and the total number of adherent cells (Figure 5). While the present data is not statistically significant due to low sample count trends can be observed in the average overall cell number. In total the experiment was carried out four times. While only a small increase in total number of adherent cells can be seen for small distances of 200 nm (A1) in contrast to the flat reference surface (A0), actually a decrease can be seen if the pillar distance is then further increased to 300 nm (A2) or 400 nm (A3) ($p = 0.14$). In case of 400 nm interpillar distances (A3) a reduction of up to 50% can be observed. This trend is also visible in the 24 h incubation time results. The biggest difference can be observed between A1 and A3 (2 h: $p = 0.14$; 24 h: $p = 0.08$). Though the small sample

number limits the significance drastically the trend can be repeatedly observed for all individual measurement. In general the observed trend follows the observations which have been found earlier on PET nanopillars [4].

The mechanisms of the observed reduction of the total number of adherent bacteria can have different reasons. One possible reason is that the degree of deformation of the cell membrane of gram negative *E. coli* strain can influence the theoretical results drastically. If the expected value (red line in Figure 5) was reached completely it would mean that all available contact area on top of the pillars beneath one single bacterium would be completely occupied by the bacterium. This could only be possible if the cell membrane would allow a complete deformation to a fully flattened shape which is neither realistic nor physically possible except for a rupture of the cell membrane and thereby a dead bacterium.

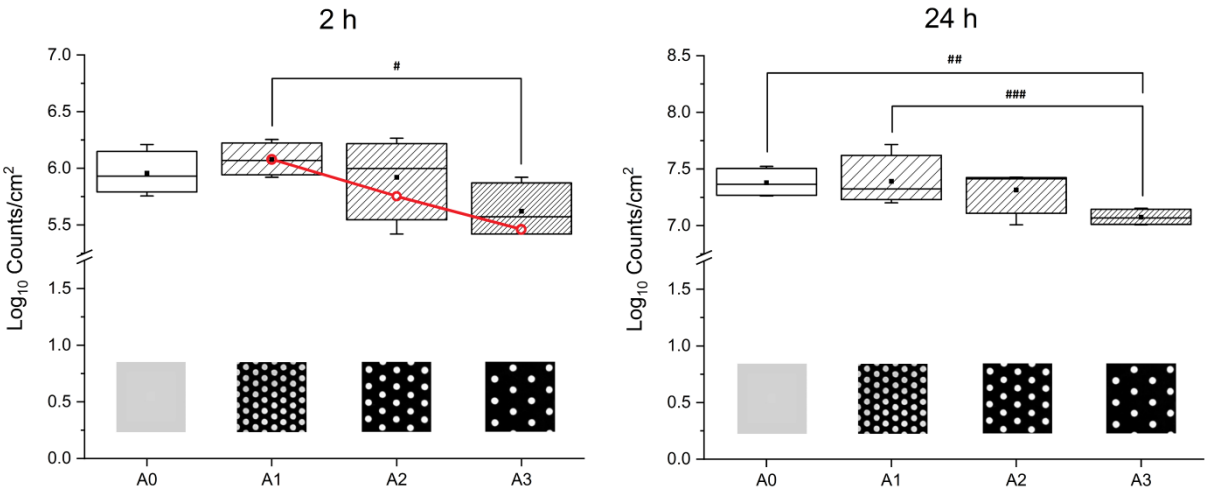


**Figure 4:** Results of the quantitative cell analysis of initial adhesion after 2h and after 24 h of incubation. Both diagrams indicate trends towards a slight reduction of the total number of adherent bacteria as the pillar distance increase. (# p=0.14; ## p=0.10; ### p=0.08) The red line in the 2 h incubation diagram indicates the estimated values nominalized to A1 which were expected by simple reduction of available contact area by increasing the pillar distances.

*3.2.2. Cell Orientation*

Results show that while there is no alignment of cells to the flat reference samples, the alignment to the hexagonal pattern of the pillar arrays increases with increasing interpillar distance. **Figure 6** shows that behavior. As generally expected this alignment can also be seen for small interpillar distance of only 200 nm. In respect to the pillar diameter of 100 nm a

sidewall to sidewall gap of 100 nm is present. The result of alignment of the cells at this distance can be divided into 6 main groups of different angles of orientation. For the 300 nm interpillar distance (resulting in a 200 nm sidewall to sidewall gap) the main orientations of 0° and 30° can already be recognized though other orientations are still present. For the largest interpillar distance of 400 nm and therefore a resulting gap of 300 nm nearly all cells align to the interpillar space resulting in only 4 major orientation groups namely 0, 30, 60 and 90°. An observation which can be seen for a majority of the samples is that cells align within the interpillar space and not on top of only one line of pillar as Figure 6, b, c indicates. This behavior results in a maximum surface contact for individual bacteria what means that cells tend to adhere to the largest possible surface area available what might allow them to form tighter bonds. On the other hand this finding also allows assumptions on the non-adherent or only weak adherent cells lying on top of the structures which maybe have been washed away due to lowered bond strength. Yet this behavior has to be investigated further to prove such an assumption.

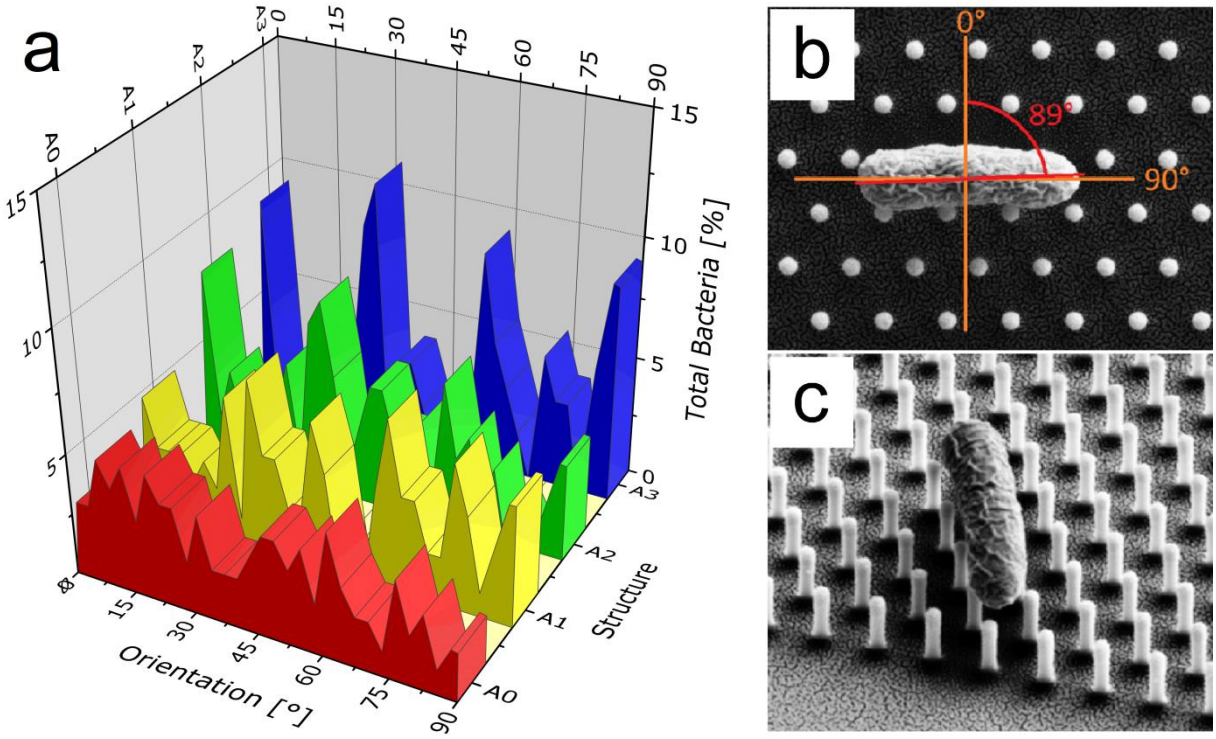


**Figure 5:** a) Diagram of alignment of rod shaped *E. coli* to nanopillar arrays. The alignment of the bacteria to the pillar pattern increases with increasing pillar distance (A0 to A3). For the

largest distance of 400 nm nearly all cells are fully aligned to the pillar pattern as the four major peaks indicate. Alignment is observed to be mainly between two rows of pillars and not on top of just one row of pillars. b) SEM image of a cell which aligned to the interpillar space between two rows of pillars resulting in an orientation angle of approx. 89°. c) Tilted SEM image of an aligned bacterium oriented approx. 30° between two rows of pillars.

Both results of quantitative cell analysis and cell orientation show the potential of the fabrication technology to investigate and to modify the initial bacteria adhesion on biomaterials.

Due to increasing antibiotic resistance against a wide range of clinically used antibiotics after the discovery of penicillin in 1928, a golden era of antibiotics began in the 1940s and lasted until the end of 1960s [38, 39]. From the 1970s until now a lack of new classes of antibiotics threatens to come back into the pre-antibiotic era [40, 41]. This stresses the need for new strategies such as the fabrication of surfaces with nanopillar arrays to avoid infections in hospitals. It should be emphasized that more than 60% of all microbial infections in communities and hospitals are caused by biofilms [42]. If the initial adhesion which depicts the first step of biofilm formation is prevented or reduced, the biofilm formation will be also prevented and diminished. This would e.g. reduce severe consequences and outcomes not only in implant surgery.

## 4. Conclusions

Within this work we could demonstrate the fabrication of different nanopillar arrays for advanced cell interaction studies. 100, 50 and 20 nm pillar arrays were fabricated by EBL in combination with RIE. By using HSQ, a negative tone high resolution photoresist, a precise structuring of the photo resist layer by exposure using an electron beam can be performed. This structured photoresist layer might be directly used for cell substrate interaction studies after development since the result of this fabrication step is a chemically stable glass like layer. Alternatively a further reactive ion etching step can be performed to create silicon nanopillars with aspect ratio of e.g. 5 or 10. By optimization of the EBL exposure parameters in form of beam current (beam diameter) and beam step size a drastic reduction of necessary

total exposure time can be achieved while the loss of detail of the pillars profile is not vast at all.

By performing cell adhesion studies with *E. coli* we could demonstrate the influence of highly ordered nanostructures on the adhesion and the alignment behavior of the rod shaped Gram-negative bacteria strain. A decreasing trend in total number of adherent cells can be correlated with the available contact area in form of discrete contact (bond) points. If the distance is in the region of cell diameter a minimum number of adherent cells can be observed while for closer distances (e.g. 200 nm) the number of adherent bacteria is higher. Additionally an alignment of cells takes place and cells tend to orientate between the pillar rows searching for maximum contact. This orientation of the bacteria to the interpillar space allows assumptions of the interactions of the bacteria with their environment. As SEM analysis indicates bacteria align to the structures with a maximum contact most of the times. This means that cells will nearly always stick between pillar rows instead of just sit on top of the pillars or pillar rows. Additionally only very few bacteria were directed into out-of-plane direction. This behavior has to be further investigated but we are confident that one can find the discrete value of possible contact area/adhesion (bond) points where bacteria can just settle down and form mechanically stable bonds instead of being washed away. A reduction of the diameter of the pillars might further decrease bacterial adhesion or may even act as a possibility for realizing contact killing surfaces. Such knowledge will allow engineers to create novel nano-textured surfaces which will reduce the bacterial adhesion to it drastically. The microbial adhesion on these new surfaces should be evaluated in extended studies of a high diversity of pathogens. *In situ* studies would reflect the real situations e.g. within the oral cavity to simulate the infections of oral implants. Single cell force spectroscopy can reveal the real adhesion forces of an individual cell to the nanostructures.

In summary we conclude that E-Beam lithography in combination with dry etching is a powerful tool for the investigation of cell substrate interaction and to create further knowledge

of the still not fully understood adhesion mechanisms of microorganisms to their environment. Such studies will lead to the devolvement to novel surfaces with superior antibacterial/antiadhesive and anti-biofilm properties.

**Acknowledgements**

The Authors thank Ms. L. Römling and Mr. G. Papagno for their excellent technical help. This work has been funded by the German Federal Ministry of Economics and Energy (BMWi) within the Innovation Program ZIM for small and middle size companies (No. KF2308206KJ4). Authors state no conflict of interest. This work has been supported by KNMF – Karlsruhe Nano Micro Facility.

**References**

[1] Chambless J D, Hunt S M, Stewart P S 2006 *Appl. Environ. Microbiol*. **72** 3

[2] Donlan R M 2001 *Clinical Infection Diseases* **33** 1387-92

[3] Høiby N 2017 *APMIS* **125** 4 272-275

[4] Jin L, Guo W, Xue P, Gao H, Zhao M, Zheng C, Zhang Y, Han D 2015 *Nanotechnology* **26** 055702

[5] Luan Y, Liu S, Pihl M, van der Mei H C, Liu J, Hizal F, Choi C-H, Chen H, Ren Y, Busscher H J 2018 *Current Opinion in Colloid & Interface Science*, DOI: 10.1016/j.cocis.2018.10.007

[6] Crawford R J, Webb H K, Truong V K, Hasan J, Ivanova E P 2012 *Adv. Colloid Interface Sci.* **1** 179-182 142-9

[7] Ivanova E P, Hasan J, Webb H K, Gervinskas G, Juodkazis S, Truong V K, Wu A H F, Lamb R N, Baulin V A, Watson G S, Watson J A, Mainwaring D E, Crawford R J 2013 *Nature Communications* **4** 2838

[8] Morton K J, Nieberg G, Bai S, Chou S Y 2008 *Nanotechnology* **19** 345301

[9] Harding F J, Surdo S, Delalat B, Cozzi C, Elnathan R, Gronthos S, Voelcker N H, Barillaro G 2016 *ACS Appl. Mater. Interfaces* **8** 43 29197-29202

[10] Kirchner T B, Hatab N A, Lavrik N V, Sepaniak M J 2013 *Anal. Chem.* **85** 24 11802-11808

[11] Jeon D-W, Choi W M, Shin H-J, Yoon S-M, Choi J-Y, Jang L-W, Lee I-H 2011 *Journal of Materials Chemistry* **21** 12688

[12] Hsu C-H, Wu R-J, Lu Y-T, Flood D J, Barron A R, Chen L C 2014 *Materials Science in Semiconductor Processing* **25** 2-17

[13] Brüggemann D, Michael K E, Wolfrum B, Offenhäuser A 2012 *Int. J. Nano and Biomaterials* **4** 2

[14] Xie C, Hanson L, Cui Y, Cui B 2011 *Proc Nat. Acad. Sci*. **108** 10

[15] Hsu C-M, Connor S T, Tang M X, Cui Y 2008 *Applied Physics Letters* **93** 133109

[16] Guerfi Y, Carcenac F, Larrieu G 2013 *Microelectonic Engineering* **1120** 173-176

[17] Song L, Wang K, Li Y, Yang Y 2016 *Colloids and Surfaces B: Biointerfaces* **148** 49-58

[18] Mills E, Cannarella J, Zhang Q, Bhadra S, Arnold C B, Chou S Y 2014 *Journal of Vacuum Science & Technology B* **32** 06FG10

[19] Rizal B, Ye F, Dhakal P, Chiles T C, Shepard S, McMahon G, Burns M J, Naughton M J 2012 *NATO Science for Peace and Security Series B: Physics and Biophysics* Springer Dordrecht

[20] Röhrig M, Schneider M, Etienne G, Oulhadj F, Pfannes F, Kolew A, Worgull M, Hölscher H 2013 *J. Micromech. Microeng.* **23** 105014

[21] Rizzello L, Cingolani R, Pompa P P 2013 *Nanomedicine* **8** 5

[22] Grainger D W, van der Mei H C, Jutte P C, van den Dungen J J, Schultz M J, van der Laan B F, Zaat S A, Busscher H J 2013 *Biomaterials* **34** 37 9237-43

[23] Garrett T R, Bhakoo M , Zhang Z 2008 *Progress in Natural Science* **18** 9 1049-1056

[24] Tuson H H, Weibel D B 2013 *Soft Matter* **9** 4368-4380

[25] Whitehead K A, Colligon J, Verran J 2005 *Colloids and Surfaces B: Biointerfaces* **25** 129-138

[26] Grigorescu A E, Hagen C W 2009 *Nanotechnology* **20** 292001

[27] Trellenkamp S, Moers J, van der Hart A, Kordos P, Lüth H 2003 *Microelectronic Engineering* **67–68** 376–380

[28] Manheller M, Trellenkamp S, Waser R, Karthäuser S 2012 *Nanotechnology* **23** 125302

[29] Yang J K W, Cord B, Duan H, Berggren K K, Klingfus J, Nam S-W, Kim K-B, Rooks M J 2009 *Journal of Vacuum Science & Technology B* **27** 6

[30] Nam S W, Rooks M J, Yang J K W, Berggren K K, Kim H-M, Lee M-H, Kim K, Sim J H, Yoon D Y 2009 *Journal of Vacuum Science & Technology B* **27** 2635

[31] Yang J K W, Berggren K K 2007 *Journal of Vacuum Science & Technology B* **25** 6

[32] Zhou J, Ji H, Lan T, Yan J, Zhou W, Miao X 2015 *Journal of Electronic Materials* **44** 1

[33] Walker M J 2001 *Proc. SPIE 4407 MEMS: Design, Fabrication, Characterization, and Packaging*, DOI:10.1117/12.425288

[34] Jones D, Pell P A, Sneath P H A 1991 *Maintenance of microorganisms and cultured cells: a manual of laboratory methods*, Academic Press London GB

[35] Al-Ahmad A, Wiedmann-Al-Ahmad M, Carvalho C, Lang M, Follo M, Braun G, Wittmer A, Mülhaupt R, Hellwig E 2008 *J. Biomed. Mater. Res.* A **87** 933-943

[36] Hochbaum A I, Aizenberg J 2010 *Nano Letter* **10** 3717–3721

[37] Verran J, Packer A, Kelly P, Whitehead K A 2010 *Letters in Applied Microbiology* **50** 258–263

[38] Laxminarayan R, Matsoso P, Pant S, Brower C, Røttingen J A, Klugman K, Davies S 2016 *Lancet* **387** 168–175

[39] Holmes A H, Moore L S P, Sundsfjord A, Steinbakk M, Regmi S, Karkey A, Guerin P J, Piddock L J V 2016 *Lancet* **387** 176–187

[40] Aminov R I 2010 *Front. Microbi*. **1** 134

[41] Lewis K 2012 *Nature* **485** 439–440

[42] Lewis K 2001 *Antimicrob. Agents Chemother*. **45** 999–1007